A Stability Analysis Tool for Bulk Power Systems Using Black-Box Models of Inverter-based Resources

Dongsen Sun
GE Global Research
1 Research Circle
Niskayuna, NY 12309, USA
Dongsen.sun@ge.com

Hanchao Liu
GE Global Research
1 Research Circle
Niskayuna, NY 12309, USA
hanchao.liu@ge.com

Maozhong Gong
GE Global Research
1 Research Circle
Niskayuna, NY 12309, USA
maozhong.gong@ge.com

***Abstract* -- This paper presents a small-signal stability analysis tool for large-scale power systems with high penetration of inverter-based resources (IBRs). Firstly, a network transfer function matrix (NTFM), which represents the information of the system topology, transmission lines, loads, IBRs locations, etc., is derived to model the entire power system network. Secondly, small-signal perturbation method is applied to obtain the sequence impedance/admittance responses of IBRs considering the frequency cross-coupling effects. With the obtained NTFM as well as IBRs' models, a multi-input, multi-output (MIMO) feedback system is constructed, and the generalized Nyquist criterion (GNC)-based stability method is employed to analyze the stability of the entire power system. Different testing cases based on a modified IEEE-14 bus system are leveraged to verify the proposed stability analysis tool.**

***Index Terms*--Black-box model, generalized Nyquist criterion (GNC), Inverter-based resources (IBRs), impedance/admittance model, stability analysis**

I. INTRODUCTION

Modern power systems have a large shares of distribution energy resources (DERs), such as renewables, electrical vehicles, energy storage, etc. As most DREs are interfaced to grid by inverters, these resources are also referred as inverter-based resources (IBRs). Due to the characteristics of the power electronics-based systems, such as low inertia as well as complex dynamics, the increased IBRs integrations could cause the stability issue of the entire power system. As described in [1], the IBRs may cause oscillations to the system with wide range of frequencies, which eventually challenges the entire system's stable operation.

In recent years, many efforts have been focusing on developing effective methods to analyze the stability of power systems with IBRs. Most existing work simplify the system to a point-to-point connection system, i.e., source-load system, and apply Nyquist criterion-based methods to analyze the system's stability [2]-[4]. Y. Li et al. [5] proposed a stability analysis and location optimization method for multi-converter power systems. W. Cao [6] proposed a component connection method to model multi-bus power systems and convert the system to a multi-input, multi-out (MIMO) for stability analysis.

However, all the existing stability analysis methods need the open-box model of IBRs, i.e., having the knowledge of control schemes as well as all parameters of IBRs, to conduct the stability analysis [2-6]. While during the power system planning studies, manufacturers would only provide the black-box models of IBRs and not disclose details on the control system architecture and parameters. Thus, it is necessary to develop a stability analysis tool which could be applied for the power systems studies with black-box IBRs.

To fill the above-discussed technical gap, this paper presents the development of the small-signal stability analysis tool for bulk power systems with a high-level integration of IBRs. Furthermore, the proposed tool directly uses the measured impedance from black-box models instead of using analytical models, which reduces the implementation complexity and improves the feasibility of the system stability analysis.

The remainder of this paper is organized as follows. Section II presents the detailed small-signal modeling of the power systems including the network transfer function matrix (NTFM) as well as the black-box models of IBRs (including models of grid-forming (GFM) and grid following (GFL) inverters). Sections III presents how the power system is converted to a MIMO feedback system and the GNC is applied to conduct the stability analysis. Section IV shows case study and validates the effectiveness of the proposed methods. Finally, Section V summarizes the paper and draws the conclusion.

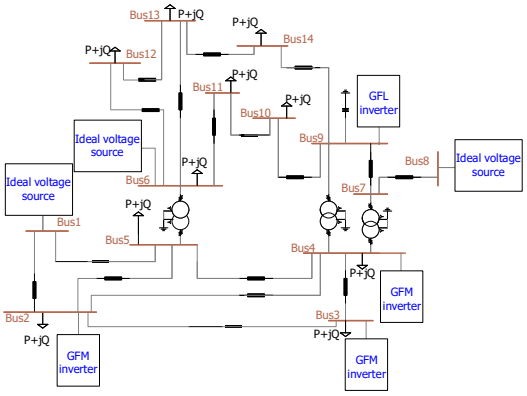

Fig. 1. An example power system network with multiple IBRs.

II. MODELING OF THE POWER SYSTME NETWORK

A. Network Transfer Function Matrix

To elaborate the development procedure of the system stability analysis tool, a modified IEEE-14 bus power system

This work is supported by the U.S. Department of Energy's Office of Energy Efficiency and Renewable Energy (EERE) under the Solar Energy Technologies Office Award Number DE-EE0009024.

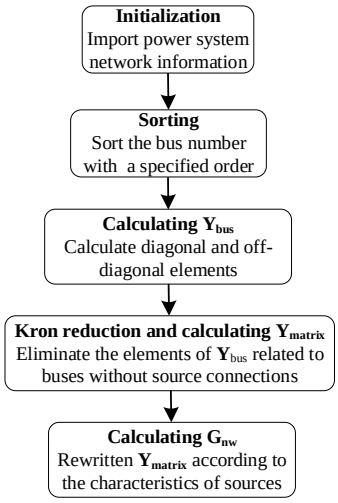

Fig. 2. Flow chart of calculating NTFM $\mathbf{G}_{nw}$.

[7] with multiple IBRs is used an example, as shown in Fig. 1. In the system, there are three GFM inverters connected to Bus 2, 3 and 4, respectively; one GFL inverter connected to Bus 9; and three ideal voltage sources (IVS) connected to Bus 1, 6 and 8, respectively.

Without considering the IBRs or IVSs, NTFM $\mathbf{G}_{nw}(s)$ of the power system is derived in this section and the detailed procedure is shown as a flowchart in Fig. 2 [6], [8]. Firstly, the specification of the power system network, including power rating, voltage rating, loads, transmission lines, source on each bus, is imported and initialized from input files. Then, $\mathbf{Y}_{bus}(s)$ is generated with a special order per the characteristic of the source on each bus. In this paper, the GFM and GFL inverters are modeled as Thevenin equivalent voltage sources and Norton equivalent current sources, respectively. While IVSs are modeled as an ideal voltage source. Thus, there is

$$\mathbf{I} = \mathbf{Y}_{\mathrm{bus}}(s)\,\mathbf{V} \tag{1}$$

where $\mathbf{V}$ is the bus voltage vector, $\mathbf{V}$= [V_1, V_2, V_3, V_4, V_6, V_8, V_9, V_5, V_7, V_{10}, V_{11}, V_{12}, V_{13}, V_{14}]; $\mathbf{I}$ is the current vector, which represents the current injected to each bus and has the same order as $\mathbf{V}$. Note that the load on the bus is converted to an admittance during obtaining the corresponding elements of $\mathbf{Y}_{bus}(s)$.

Moreover, $\mathbf{Y}_{bus}(s)$ should be expressed in a positive and negative sequence format to be compatible with the sequence impedance/admittance model of IBRs in the following section. There is

$$\mathbf{Y}_{\mathrm{bus}}(s) = \begin{bmatrix} \mathbf{Y}_{pp11} & \mathbf{Y}_{pn11} & \mathbf{Y}_{pp12} & \mathbf{Y}_{pn12} & \cdots & \cdots \\ \mathbf{Y}_{np11} & \mathbf{Y}_{nn11} & \mathbf{Y}_{np12} & \mathbf{Y}_{nn12} & \cdots & \cdots \\ \mathbf{Y}_{pp21} & \mathbf{Y}_{pn21} & \cdots & \cdots & \cdots & \cdots \\ \mathbf{Y}_{np21} & \mathbf{Y}_{nn21} & \cdots & \cdots & \cdots & \cdots \\ \cdots & \cdots & \cdots & \cdots & \cdots & \cdots \\ \cdots & \cdots & \cdots & \cdots & \cdots & \cdots \end{bmatrix} \tag{2}$$

where subscripts p and n denote the positive and negative sequence, respectively. $\mathbf{Y}_{ppnn}$, $\mathbf{Y}_{pnnn}$, $\mathbf{Y}_{npnn}$, and $\mathbf{Y}_{nnnn}$ are the positive and negative sequence components of the nn^{th} element of $\mathbf{Y}_{bus}$, respectively.

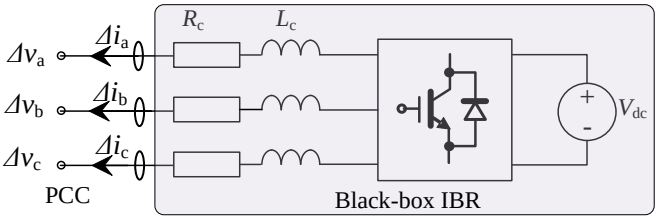

Fig. 3. Schematic diagram of small-signal perturbation method to measure the black-box IBR model.

To eliminate the elements of $\mathbf{Y}_{bus}$ related to the buses without source connected, Kron reduction needs to be conducted [6], [8] on $\mathbf{Y}_{bus}$. Firstly, equation (1) is rewritten as

$$\begin{bmatrix} \mathbf{I}_m \\ \mathbf{I}_n \end{bmatrix} = \begin{bmatrix} \mathbf{Y}_{mm}(s) & \mathbf{Y}_{mn}(s) \\ \mathbf{Y}_{nm}(s) & \mathbf{Y}_{nn}(s) \end{bmatrix} \begin{bmatrix} \mathbf{V}_m \\ \mathbf{V}_n \end{bmatrix} \tag{3}$$

where subscripts m and n represent the buses with and without source, respectively. Thus, we have $\mathbf{V}_m$= [V_1, V_2, V_3, V_4, V_6, V_8, V_9] and $\mathbf{V}_n$= [V_5, V_7, V_{10}, V_{11}, V_{12}, V_{13}, V_{14}].

After conducting Kron reduction, there is

$$\mathbf{I}_m = \mathbf{Y}_{\mathrm{matrix}}(s)\,\mathbf{V}_m \tag{4}$$

$$\mathbf{Y}_{\mathrm{matrix}}(s) = \mathbf{Y}_{mm}(s) - \mathbf{Y}_{mn}(s)\,\mathbf{Y}_{nn}(s)^{-1}\mathbf{Y}_{nm}(s) \tag{5}$$

According to the characteristic of the source on each bus, equation (4) is rewritten as

$$\begin{bmatrix} \mathbf{I}_v \\ \mathbf{I}_c \end{bmatrix} = \begin{bmatrix} \mathbf{Y}_{vv}(s) & \mathbf{Y}_{vc}(s) \\ \mathbf{Y}_{cv}(s) & \mathbf{Y}_{cc}(s) \end{bmatrix} \begin{bmatrix} \mathbf{V}_v \\ \mathbf{V}_c \end{bmatrix} \tag{6}$$

where subscripts v and c represent the voltage- and current-controlled voltage sources, respectively. Thus, $\mathbf{V}_v$= [V_1, V_2, V_3, V_4, V_6, V_8] and $\mathbf{V}_c$= [V_9].

Finally, $\mathbf{G}_{nw}(s)$ is obtained as

$$\begin{bmatrix} \mathbf{I}_v \\ \mathbf{I}_c \end{bmatrix} = \mathbf{G}_{\mathrm{nw}}(s) \begin{bmatrix} \mathbf{V}_v \\ \mathbf{I}_c \end{bmatrix} \tag{7}$$

$$\mathbf{G}_{\mathrm{nw}}(s) = \begin{bmatrix} \mathbf{Y}_{vv} - \mathbf{Y}_{vc}\mathbf{Y}_{cc}^{-1}\mathbf{Y}_{cv} & \mathbf{Y}_{vc}\,\mathbf{Y}_{cc}^{-1} \\ -\mathbf{Y}_{cc}^{-1}\mathbf{Y}_{cv} & \mathbf{Y}_{cc}^{-1} \end{bmatrix} \tag{8}$$

B. Black-box Model of IBRs

As the IBRs in the power system network are mostly black boxes without detailed internal information, it is necessary to obtain their impedance/admittance model using measuring method. Fig. 3. shows the schematic diagram of the measuring method. In this figure, small-signal positive and negative voltage perturbations with different frequency is applied at the point of common coupling (PCC) between the IBR and its connecting bus.

The current corresponding to the applied voltage perturbation can be measured, and then using fast Fourier transform (FFT) calculation, the impedance/admittance model of GFM/ GFL inverter can be obtained. Due to the space limit, the details of obtaining the measured model are not presented here, and more information could be referred to [9].

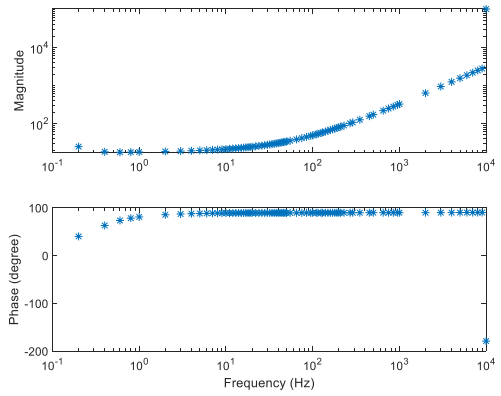

(a) Z_{pp}

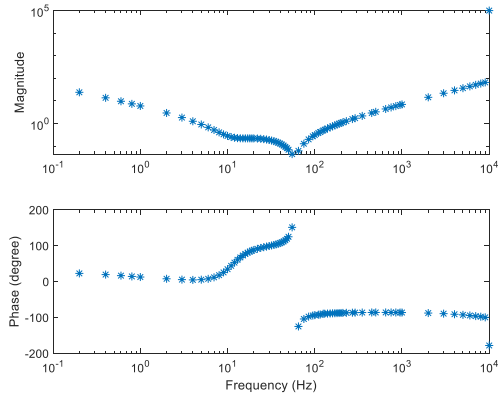

(b) Z_{pn}

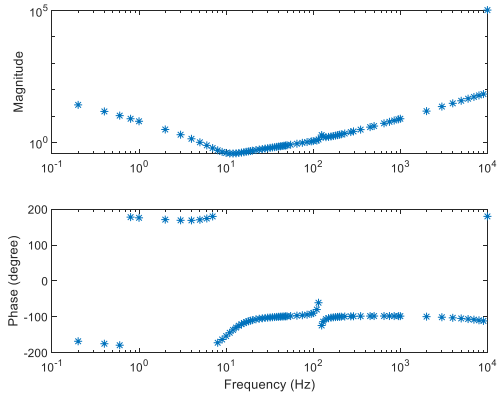

(c) Z_{np}

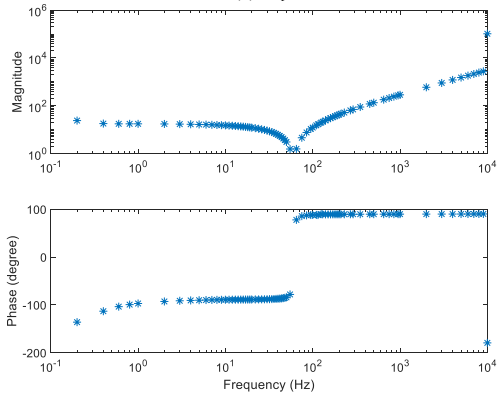

(d) Z_{nn}

Fig. 4. Impedance model of a GFM inverter.

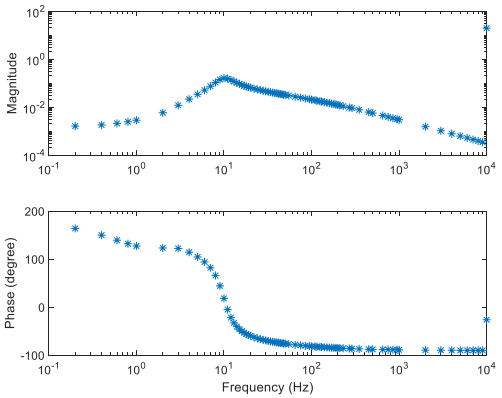

(a) Y_{pp}

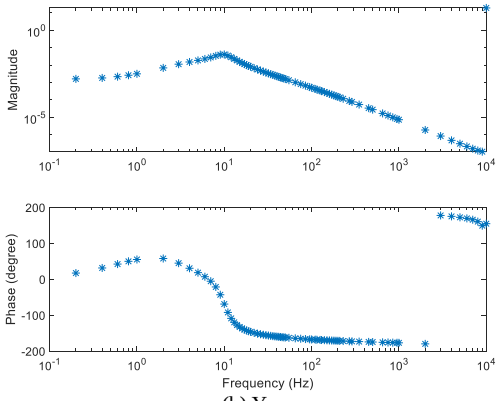

(b) Y_{pn}

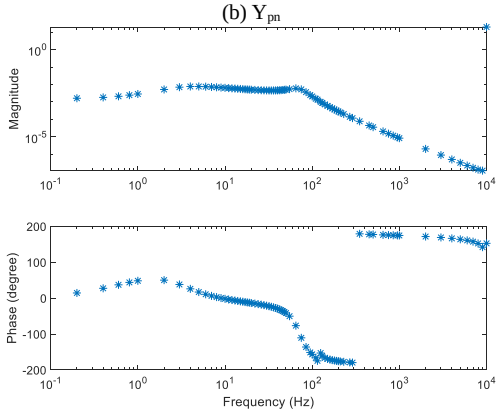

(c) Y_{np}

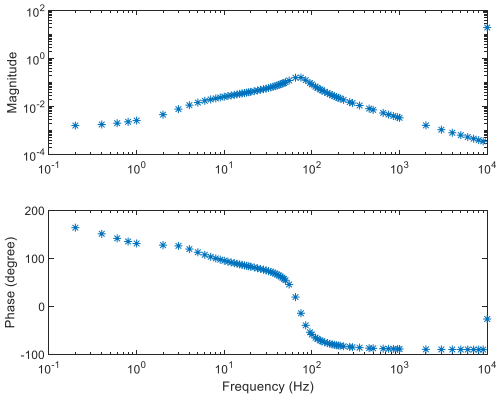

(d) Y_{nn}

Fig. 5. Admittance model of a GFL inverter.

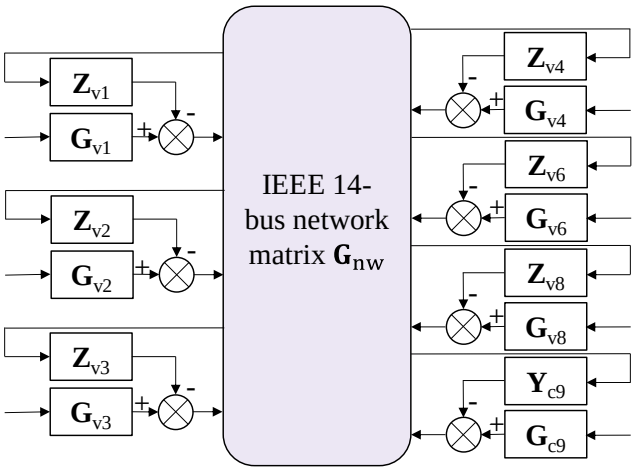

Fig. 6. Constructed MIMO feedback system of the whole system.

Figs. 4 and 5 show the measured sequence impedance model of a GFM inverter and the measured sequence admittance model of a GFL inverter, respectively. Thus, the measured black-box model of GFM and GFL inverters can be expressed as

$$\mathbf{Z}_{\mathrm{v}}(\mathrm{s}) = \begin{bmatrix} \mathbf{Z}_{\mathrm{pp}} & \mathbf{Z}_{\mathrm{pn}} \\ \mathbf{Z}_{\mathrm{np}} & \mathbf{Z}_{\mathrm{nn}} \end{bmatrix} \tag{9}$$

$$\mathbf{Y}_{\mathrm{c}}(\mathrm{s}) = \begin{bmatrix} \mathbf{Y}_{\mathrm{pp}} & \mathbf{Y}_{\mathrm{pn}} \\ \mathbf{Y}_{\mathrm{np}} & \mathbf{Y}_{\mathrm{nn}} \end{bmatrix} \tag{10}$$

where $\mathbf{Z}_{\mathrm{pp}}(\mathbf{Y}_{\mathrm{pp}})$, $\mathbf{Z}_{\mathrm{pn}}(\mathbf{Y}_{\mathrm{pn}})$, $\mathbf{Z}_{\mathrm{np}}(\mathbf{Y}_{\mathrm{np}})$, and $\mathbf{Z}_{\mathrm{nn}}(\mathbf{Y}_{\mathrm{nn}})$ are the corresponding positive and negative sequence impedance (admittance) components, respectively.

III. GNC-BASED STABILITY ANALYSIS

With the obtained system network model $\mathbf{G}_{\mathrm{nw}}(\mathrm{s})$ as well as all the IBRs' models, a MIMO feedback system is constructed as shown in Fig. 6. In the figure, $\mathbf{G}_{\mathrm{v}n}(\mathrm{s})$ (n=1, 2, 3, 4, 6, 8) and $\mathbf{G}_{\mathrm{c}m}(\mathrm{s})$ (m=9) are the closed-loop gain of the GFM inverter and GFL inverter based IBRs, respectively. Moreover, $\mathbf{Z}_{\mathrm{v}n}(\mathrm{s})$ (n=1, 2, 3, 4, 6, 8) and $\mathbf{Y}_{\mathrm{c}m}(\mathrm{s})$ (m=9) represent the measured output impedance of GFM inverter and the measured output admittance of GFL inverter, respectively.

Writing all the measured models of the IBRs as a matrix, there is

$$\mathbf{G}_{\mathrm{cd}}(\mathrm{s}) = \mathrm{diag}[\mathbf{Z}_{\mathrm{v1}}, \mathbf{Z}_{\mathrm{v2}}, \mathbf{Z}_{\mathrm{v3}}, \mathbf{Z}_{\mathrm{v4}}, \mathbf{Z}_{\mathrm{v6}}, \mathbf{Z}_{\mathrm{v8}}, \mathbf{Y}_{\mathrm{c9}}] \tag{11}$$

Moreover, to conduct stability analysis of the MIMO feedback system, the return-ratio matrix $\mathbf{L}(\mathrm{s})$ and the return-difference matrix $\mathbf{F}(\mathrm{s})$ are defined as

$$\mathbf{L}(\mathrm{s}) = \mathbf{G}_{\mathrm{cd}}(\mathrm{s})\,\mathbf{G}_{\mathrm{nw}}(\mathrm{s}) \tag{12}$$

$$\mathbf{F}(\mathrm{s}) = \mathbf{I} + \mathbf{L}(\mathrm{s}) \tag{13}$$

According to the GNC, the stability of the constructed MIMO system can be analyzed by two methods, one is the determinant-based method, and the other is the eigenvalue-based method.

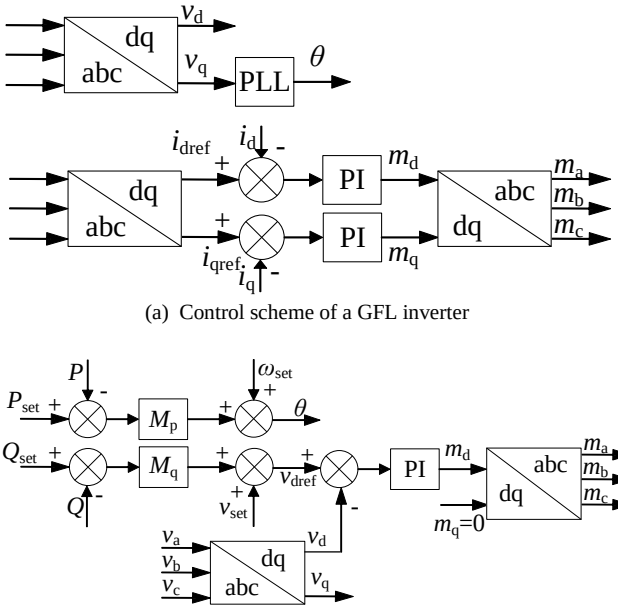

(a) Control scheme of a GFL inverter

(b) Control scheme of a GFM inverter

Fig. 7. Control scheme of IBRs in the power system

Defining that $\boldsymbol{Z}$ is the number of zeros of $\mathbf{F}(\mathrm{s})$, $\boldsymbol{P}$ is the number of right-half-plane (RHP) poles of $\mathbf{L}(\mathrm{s})$, and $\boldsymbol{N}$ is the number of clockwise encirclements of the critical point ((0, j0) for determinant-based method and (-1, j0) for eigenvalue-based method), according to the GNC [6], [10], there is

$$\boldsymbol{Z}(\mathbf{F}) = \boldsymbol{P}(\mathbf{L}) + \boldsymbol{N}(\mathbf{L}) \text{ or } \boldsymbol{Z}(\mathbf{F}) = \boldsymbol{P}(\mathbf{L}) + \boldsymbol{N}(\det(\mathbf{F})) \tag{14}$$

As the power system network consists only passive components, there is no RHP poles on $\mathbf{G}_{\mathrm{nw}}(\mathrm{s})$. Moreover, all the IBRs are designed to operate stably with ideal conditions, so there is no RHP poles on $\mathbf{G}_{\mathrm{cd}}(\mathrm{s})$. Therefore, $\mathbf{L}(\mathrm{s})$ does not have any RHP poles, i.e., $\boldsymbol{P}(\mathbf{L})$=0. Thus, the system is stable if and only if

1) the Nyquist plot of $\det(\mathbf{F}(\mathrm{s}))$ does not encircle critical point (0, j0) clockwise.

2) the Nyquist plots of all the eigenvalue of $\mathbf{L}(\mathrm{s})$ do not encircle critical point (-1, j0) clockwise.

TABLE I
SYSTEM PARAMETERS

		Symbol	Value
GFM/GFL inverter power rating		P_{rated}	100 MW
GFM/GFL inverter rated voltage		V_{rated}	138 kV
GFM/GFL inverter circuit parameters		R_{c}	0.367 Ω
		L_{c}	0.05 H
P-f droop gain		M_{p}	0.05 p.u.
Q-V droop gain		M_{q}	0.05 p.u.
GFL inverter PLL	Case1	k_{ppll}	30
		k_{ipll}	400
	Case2	k_{ppll}	30
		k_{ipll}	165
GFL inverter current PI controller		k_{pc}	0.05
		k_{ic}	12.5
GFM inverter voltage PI controller		k_{pv}	0.05
		k_{iv}	1

IV. Case Study

A modified IEEE-14 bus system with multiple IBRs shown Fig. 1 is used to verify the proposed stability analysis tool. For easy implementation, GFM and GFL inverters are built in PSCAD with adjustable parameters, and the control schemes of the GFL and GFM inverters are shown in Fig. 7, respectively. Moreover, the corresponding sequence impedance/admittance models of the GFL and GFM inverters are measured using the method discussed in Section II.B. Two different cases are studied in this section and the system parameters are shown in Table I.

A. Case1: (unstable system)

In this case, the IEEE-14 bus power system is simulated in PSCAD with the parameters shown in Table I. The system is unstable and presents oscillations in the entire system. Fig. 8 shows the performance of the GFL inverter on Bus 9. The d- and q-axis currents of the GFL inverter are shown in Fig. 8 (a), respectively, in which the obvious oscillations around 5 Hz can be observed. Fig. 8 (b) shows the voltage and current at PCC, which also demonstrates that the system is unstable.

Fig. 9 shows the performance of the GFM inverter on Bus 4. Fig. 9 (a) shows the real and reactive powers of the GFM inverter, respectively. The powers also present obvious oscillations around 5 Hz. Fig. 9 (b) shows the unstable voltage and current at PCC.

Figs. 10 and 11 show the stability analysis results with the determinant- and eigenvalue-based methods, respectively. Fig. 10 shows that the Nyquist plot of det(**F**) encircles the critical point (0, j0) clockwise once, which indicates that the system is unstable. Due to the space limit, only one Nyquist plot of a critical eigenvalue of **L** is shown in Fig. 11. The figure not only shows that the Nyquist plot encircles the critical point (-1, j0) clockwise once, which indicate the system is unstable; but also displays that the plot crosses the unit circle at around 5 Hz and indicate the system will have oscillations around 5 Hz.

B. Case2: (stable system)

In this case, only the parameters of the phase-locked loop (PLL) of the GFL inverter are changed as shown in Table I, and all other parameters keep the same as case 1. With the modified parameters, the power system can operate stably.

Fig. 12 shows the performance of the GFL inverter on Bus 9. Fig. 12 (a) shows the d- and q-axis current of the GFL inverter, respectively. All the currents can track their references after a small period of oscillations. Fig. 12 (b) shows the voltage and current at PCC and indicates that the system could operate stably.

Fig. 13 shows the performance of the GFM inverter on Bus 4. Fig. 13 (a) shows the real and reactive powers of the GFM inverter, respectively, which indicates that the GFM inverter can provide constant powers in this case. Fig. 13 (b) shows the voltage and current at PCC, which also presents that the system is stable.

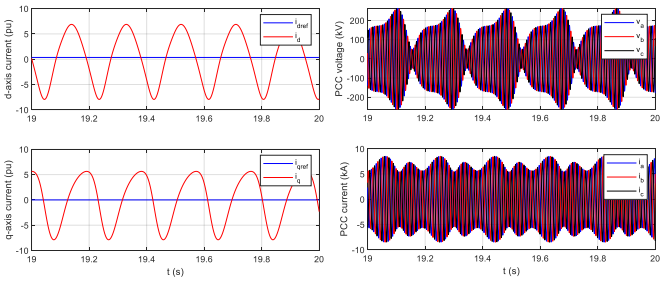

(a) d- and q-axis currents. (b) Voltage and current at PCC.

Fig. 8. PSCAD simulation result of the GFL inverter on Bus 9.

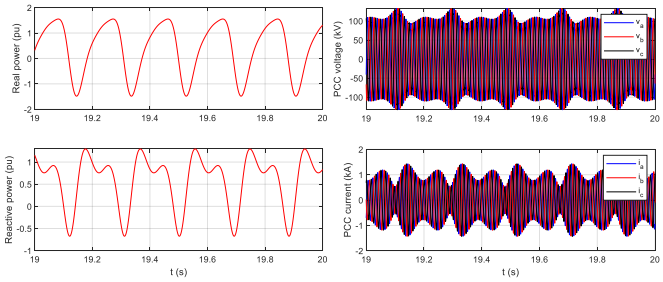

(a) Real and reactive powers. (b) Voltage and current at PCC.

Fig. 9. PSCAD simulation result the GFM inverter on Bus 4.

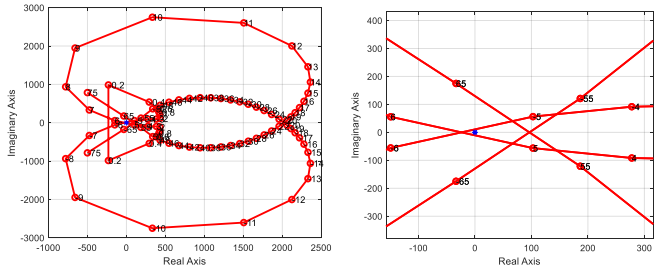

(a) Nyquist plot of det(**F**). (b) Zoomed-in view.

Fig. 10 Stability analysis result with determinant-based method.

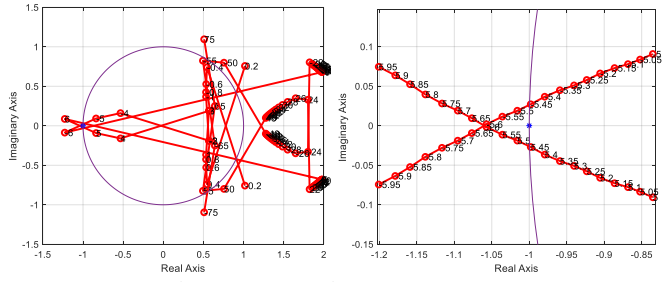

(a) Nyquist plot of the eigenvalue of **L**. (b) Zoomed-in view.

Fig. 11. Stability analysis result with eigenvalue-based method.

Fig. 14 shows the determinant- and eigenvalue-based stability analysis results, respectively. The figure shows that neither the Nyquist plot of det(**F**) nor the Nyquist plot of the eigenvalue of **L** encircles their critical points, which indicates the system is stable.

V. Conclusion

The impedance stability analysis tool using black-box model is developed in this paper to analyze bulk power systems with high level penetration of black-box IBRs. The procedure

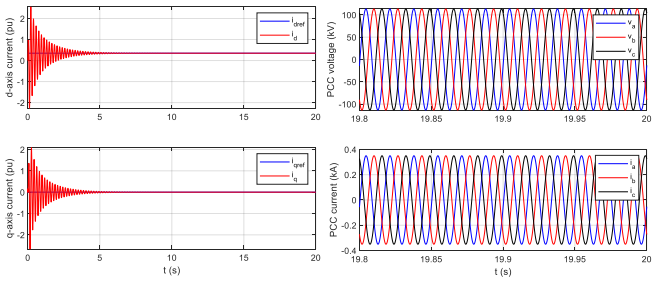

(a) d- and q-axis currents. (b) Voltage and current at PCC.

Fig. 12. PSCAD simulation result of GFL inverter on Bus 9.

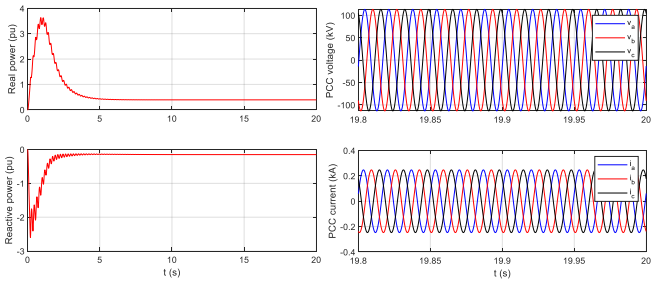

(a) Real and reactive powers. (b) Voltage and current at PCC.

Fig. 13. PSCAD simulation result of the GFM inverter on Bus 4.

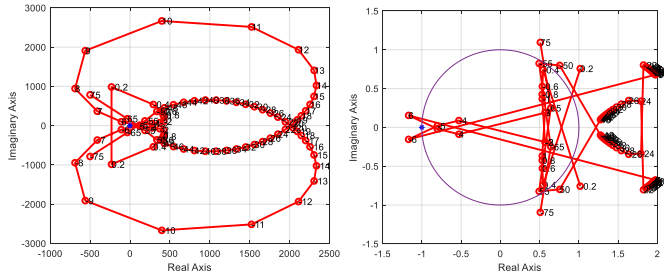

(a) Nyquist plot of det(**F**). (b) Nyquist plot of eigenvalue of **L**.

Fig. 14. Analysis result with determinant- and eigenvalue-based methods.

of conducting stability analysis of the power system network is presented in detail. Different cases based on a modified IEEE-14 bus power system are studied to validate the effectiveness of the proposed methods. The testing results show that both methods could determine if the system can operate stably with the connections of IBRs; moreover, the eigenvalue-based method could further predict the system's oscillation frequency if the system is unstable.

REFERENCES

[1] Shah, Shahil, et al. "Impedance Methods for Analyzing Stability Impacts of Inverter-Based Resources: Stability Analysis Tools for Modern Power Systems." IEEE Electrification Magazine, vol. 9, no. 1, pp. 53-65, Mar. 2021.

[2] B. Wen, D. Dong, D. Boroyevich, R. Burgos, P. Mattavelli, and Z. Shen, "Impedance-based analysis of grid-synchronization stability for three-phase paralleled converters," IEEE Trans. Power Electron., vol. 31, no. 1, pp. 26–38, Jan. 2016.

[3] M. Amin and M. Molinas, "Small-Signal Stability Assessment of Power Electronics Based Power Systems: A Discussion of Impedance- and Eigenvalue-Based Methods," IEEE Transactions on Industry Applications, vol. 53, no. 5, pp. 5014-5030, Sept.-Oct. 2017.

[4] Y. Liao and X. Wang, "Impedance-Based Stability Analysis for Interconnected Converter Systems With Open-Loop RHP Poles," IEEE Transactions on Power Electronics, vol. 35, no. 4, pp. 4388-4397, April 2020.

[5] Y. Li et al., "Stability Analysis and Location Optimization Method for Multiconverter Power Systems Based on Nodal Admittance Matrix," IEEE Journal of Emerging and Selected Topics in Power Electronics, vol. 9, no. 1, pp. 529-538, Feb. 2021.

[6] W. Cao, "Impedance-based Stability Analysis and Controller Design of Three-phase Inverter-based AC Systems," Ph.D. dissertation, University of Tennessee, Knoxville, 2017.

[7] Illinois Center for a Smarter Electric Grid. (2013). [Online]. Available FTP: http://publish.illinois.edu/smartergrid/

[8] J. Grainger and W. Stevenson, "Power system analysis," New York: McGraw-Hill, 1994, pp. 238-280.

[9] S. Shah, P. Koralewicz, V. Gevorgian and R. Wallen, "Sequence Impedance Measurement of Utility-Scale Wind Turbines and Inverters Reference Frame, Frequency Coupling, and MIMO/SISO Forms," in IEEE Transactions on Energy Conversion, doi: 10.1109/TEC.2021.3093516.

[10] S. Skogestad and I. Postlethwaite, "Multivariable feedback control: analysis and design," Hoboken, NJ: John Wiley, 2nd edition, 2005, pp.113-150.